

## Partial Dissociation of Water on Fe<sub>3</sub>O<sub>4</sub>(001): Adsorbate Induced Charge and Orbital Order

Narasimham Mulakaluri,<sup>1,2</sup> Rossitza Pentcheva,<sup>1,\*</sup> Maria Wieland,<sup>1</sup> Wolfgang Moritz,<sup>1</sup> and Matthias Scheffler<sup>2</sup>

<sup>1</sup>Department of Earth and Environmental Sciences, University of Munich, Theresienstr. 41, 80333 Munich, Germany

<sup>2</sup>Fritz-Haber-Institut der Max-Planck-Gesellschaft, Faradayweg 4-6, D-14195 Berlin, Germany

(Received 7 July 2009; published 23 October 2009)

The interaction of water with Fe<sub>3</sub>O<sub>4</sub>(001) is studied by density functional theory calculations including an on-site Coulomb term. For isolated molecules, dissociative adsorption is strongly promoted at surface defect sites, while at higher coverages a hydrogen-bonded network forms with alternating molecular and dissociated species. This mixed adsorption mode and a suppression of the ( $\sqrt{2} \times \sqrt{2}$ )R45° reconstruction are confirmed by a quantitative low energy electron diffraction analysis. Adsorbate induced electron transfer processes add a new dimension towards understanding the catalytic activity of magnetite(001).

DOI: 10.1103/PhysRevLett.103.176102

PACS numbers: 68.43.Bc, 68.35.Md, 68.47.Gh, 73.20.-r

Magnetite has attracted continued interest in the past decades due to its fascinating properties: The high temperature phase is predicted to be a half-metallic ferrimagnet [1] with a high Curie temperature (858 K). At  $\sim 120$  K it undergoes the so called Verwey transition [2]. Both the type of transition (metal-to-insulator vs semiconductor-to-semiconductor [3,4]) and the type of charge (CO) and orbital ordering (OO) at the octahedral iron sites in the low temperature phase are subject to an ongoing debate [5–8].

In addition to its applications in magnetic recording and as a prospective material for spintronics, magnetite acts as a catalyst, e.g., in environmental redox reactions [9,10], or in the water gas phase shift reaction [11]. Typically these reactions take place in an aqueous environment prompting the need to understand how water interacts with the Fe<sub>3</sub>O<sub>4</sub> surface. Water can bind to a surface in different modes (e.g., molecular or dissociative) leading to a variety of functional groups that can affect significantly the surface properties and availability of reaction sites and result in a complex surface chemistry [12,13].

The catalytic activity of magnetite is typically related to the presence of both ferrous (Fe<sup>2+</sup>) and ferric (Fe<sup>3+</sup>) iron in its inverse spinel structure. In the [001] direction two types of layers alternate: *A* layers with tetrahedral iron (Fe<sub>A</sub><sup>3+</sup>) and *B* layers containing oxygen and octahedral iron (Fe<sub>B</sub><sup>2+,3+</sup>). Both bulk truncations of Fe<sub>3</sub>O<sub>4</sub>(001), either with an *A* or a *B* layer are polar of type three according to the classification of Tasker [14]. To explain the origin of the ( $\sqrt{2} \times \sqrt{2}$ )R45° reconstruction, previous surface models proposed an ordering of surface defects (e.g., [15,16]). Recently, density functional theory (DFT) calculations [17,18] have shown that the symmetry lowering at Fe<sub>3</sub>O<sub>4</sub>(001) is achieved rather by a distorted *B* layer, supported also by surface x-ray diffraction [17], low energy electron diffraction (LEED) [19] and scanning tunneling microscopy (STM) [20].

Despite its importance, only a few studies have addressed the interaction of water with Fe<sub>3</sub>O<sub>4</sub>(001). While initial adsorption was related to surface defect sites, an

extensive hydroxylation was reported from x-ray photoemission experiments (XPS) beyond a threshold pressure of  $10^{-3}$ – $10^{-4}$  mbar [21]. Both this study and temperature programmed desorption (TPD) measurements [22] indicate multiple adsorbate sites on the surface. Molecular dynamics simulations with empirical potentials [23,24] point towards a dissociative adsorption. However, such studies cannot provide reliable information on the energetics and underlying electronic phenomena.

Here we address these fundamental questions within a combined DFT and LEED approach. By varying the coverage and adsorbate configuration of water molecules we compile a surface phase diagram in the framework of *ab initio* atomistic thermodynamics. The results show that isolated molecules dissociate on the clean Fe<sub>3</sub>O<sub>4</sub>(001) surface. This process is strongly favored at oxygen vacancies. With increasing coverage a crossover to a mixed adsorption (both molecular and dissociative) takes place that is confirmed in a quantitative LEED analysis. LEED shows also a strong suppression of the ( $\sqrt{2} \times \sqrt{2}$ )R45° surface reconstruction. Furthermore, we find that the adsorbed species invoke electron transfer processes in the subsurface layers resulting in a unique CO/OO that may have important implications on the catalytic activity of the surface.

DFT calculations were performed using the full potential linear augmented plane wave method in the WIEN2K [25] implementation. The generalized gradient approximation (GGA-PBE) [26] of the exchange-correlation potential, used here, tends to overestimate hydrogen bonding by up to 20 meV/bond [27] which does not affect our conclusions. Because magnetite is a strongly correlated material we have used an on-site Coulomb correction to the local density approximation (LDA/GGA + *U* method) [28] with *U* = 5 eV and *J* = 1 eV [29], similar to values used for bulk Fe<sub>3</sub>O<sub>4</sub> [6,7,30]. The surfaces were modeled in the supercell geometry with slabs containing seven *B* layers and six *A* layers separated by a vacuum region of 10–12 Å [31]. The positions of adsorbates and the atoms in the outer two *BA* layers were relaxed.

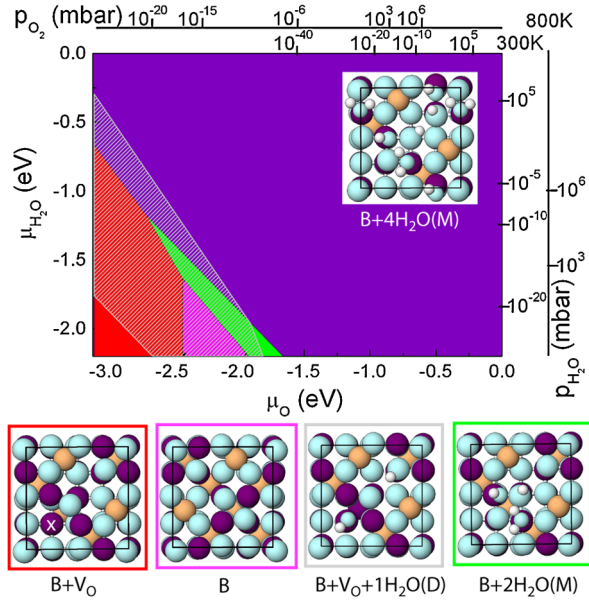


FIG. 1 (color online). Surface phase diagram of  $\text{Fe}_3\text{O}_4(001)$  showing the most stable configurations as a function of  $\mu_{\text{O}}$ ,  $\mu_{\text{H}_2\text{O}}$ :  $B + \text{V}_\text{O}$  [red (medium gray)],  $B$  layer [magenta (lighter medium gray)], dissociated molecule in an oxygen vacancy  $B + \text{V}_\text{O} + 1\text{H}_2\text{O}(D)$  (gray hatched semitransparent area), mixed adsorption of two [green (light gray)] and four water molecules on a  $B$  layer [purple (dark gray)]. The ranges of  $\mu_{\text{O}}$  and  $\mu_{\text{H}_2\text{O}}$  correspond to the vapor phase of  $\text{H}_2\text{O}$ .  $\mu_{\text{O}}$  and  $\mu_{\text{H}_2\text{O}}$  have been converted into pressures for 300 and 800 K. Additionally, the top views of the most stable configurations are displayed with positions of O,  $\text{Fe}_B$ ,  $\text{Fe}_A$  and H marked by cyan (light gray), purple (dark gray), orange (medium gray) and white circles, respectively. In  $B + \text{V}_\text{O}$  a white cross marks the position of the vacancy.

We have compared the stability of more than 30 different configurations using *ab initio* atomistic thermodynamics [32]. The surface energy,  $\gamma(T, p) = \frac{1}{2A}(G_{\text{Fe}_3\text{O}_4(001)}^{\text{slab}} - N_{\text{Fe}}\mu_{\text{Fe}} - N_{\text{O}}\mu_{\text{O}} - N_{\text{H}_2\text{O}}\mu_{\text{H}_2\text{O}})$  depends on the Gibbs free energy and the chemical potentials of the constituents. The Gibbs free energy can be expressed through the total energy from the DFT calculations [32]. Because there are two species in the gas phase,  $\text{O}_2$  and  $\text{H}_2\text{O}$ , the surface phase diagram is three dimensional. Figure 1 displays a two-dimensional projection with the most stable configurations for given  $\mu_{\text{O}}$ ,  $\mu_{\text{H}_2\text{O}}$ . We first consider the termination of the clean surface as a function of oxygen pressure. As discussed previously, a modified  $B$  layer (denoted as  $B$ ) showing lateral and vertical distortions in the surface layer with a *wavelike* pattern is favored over a broad range of oxygen pressures. However, at oxygen poor conditions a  $B$  layer with oxygen vacancies ( $B + \text{V}_\text{O}$ ) is stabilized. This defective surface, previously proposed in a STM study [16], shows dramatic relaxations where the oxygen opposite the vacancy moves towards the  $\text{Fe}_B$  row by  $\sim 0.8$  Å. Starting from these two terminations [33], we have adsorbed water molecules, varying their concentration and geometry. We find a strong tendency for isolated molecules

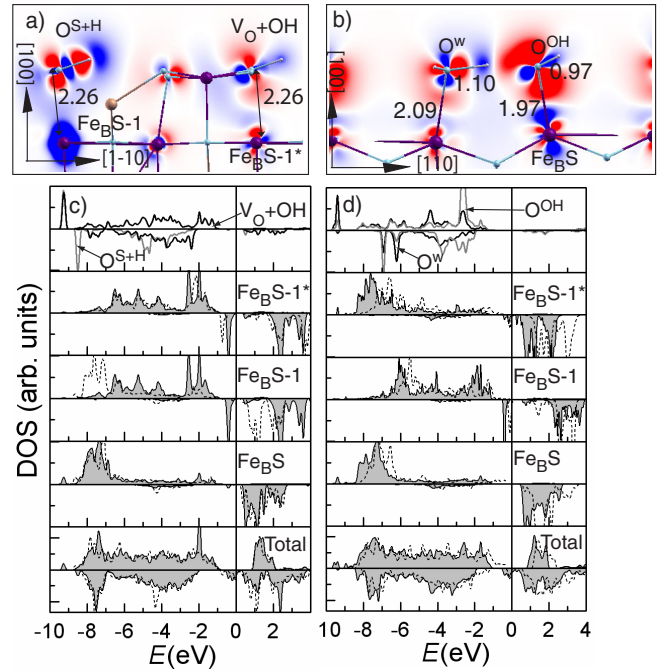


FIG. 2 (color online). Adsorbate induced electron density redistribution for (a)  $B + \text{V}_\text{O} + 1\text{H}_2\text{O}(D)$  and (b)  $B + 4\text{H}_2\text{O}(M)$ . Red (medium gray)/blue (dark gray) corresponds to regions of charge accumulation/depletion. Relevant bond lengths are given in Å. Total and projected density of states (DOS) before (dashed line) and after water adsorption (solid line, gray area) for (c)  $B + \text{V}_\text{O} + 1\text{H}_2\text{O}(D)$  and (d)  $B + 4\text{H}_2\text{O}(M)$ .  $S$  ( $S-1$ ) denote surface (subsurface)  $\text{Fe}_B$  sites.

to dissociate in surface oxygen vacancies ( $\text{V}_\text{O} + \text{OH}$ ) whereby a proton diffuses to a surface oxygen ( $\text{O}^S$ ) further away and forms a surface OH group ( $\text{O}^S + \text{H}$ ). Thus, even at very low water vapor pressures, all surface defects are expected to be filled with OH groups, consistent with XPS results [21]. As shown in Figs. 2(a) and 2(c), the dissociation of water in the defect sites invokes significant changes in the electronic structure involving the  $1\pi$  and  $3\sigma$  molecular orbitals of the OH groups and a switching from  $\text{Fe}^{3+}$  to  $\text{Fe}^{2+}$  of  $\text{Fe}_B S-1$  underneath  $\text{O}^S + \text{H}$ .

The adsorbate-adsorbate interaction that sets in, when a second molecule is adsorbed within the  $(\sqrt{2} \times \sqrt{2})R45^\circ$  unit cell, leads to a mixed adsorption mode: One molecule dissociates protonating a surface oxygen, while the intact molecule forms a hydrogen bond with the OH group. The main part of the phase diagram is dominated by a mixed adsorption mode of four water molecules where all surface  $\text{Fe}_B$  sites ( $\text{Fe}_B S$ ) are saturated ( $B + 4\text{H}_2\text{O}(M)$ ). Full dissociation is  $12 \text{ meV}/\text{Å}^2$  less stable. Full hydroxylation of the surface is also not likely to occur as the formation of a surface OH group neighboring a subsurface  $\text{Fe}_A$  is extremely unfavorable.

The electron density redistribution with respect to the  $B$  layer in Fig. 2(b) indicates a weak charge accumulation between  $\text{Fe}_B S$  and the oxygen of the water molecule ( $\text{O}^w$ ). The strongest charge rearrangement takes place between

$\text{Fe}_B$  and the OH group ( $\text{O}^{\text{OH}}$ ) of the dissociated molecule, involving depletion of  $3\sigma$  and accumulation in  $1\pi$  molecular orbitals of OH along with depletion of the  $d_{z^2}$  orbital at  $\text{Fe}_B\text{S}$ . The main actuator of partial dissociation appears to be the formation of strong intermolecular hydrogen bonds. As a result both  $\text{H}_2\text{O}$  and OH tilt from the on-top position towards each other and  $\text{O}^w\text{-H}$  elongates from 0.95 Å (gas phase) to 1.10 Å, resulting in an  $\text{O}^w\text{-H}\cdots\text{O}^{\text{OH}}$  of 2.47 Å. The two distinct bond lengths between  $\text{Fe}_B\text{-O}^w$  and  $\text{Fe}_B\text{-O}^{\text{OH}}$  of 2.09 Å and 1.97 Å, respectively, are a fingerprint of the mixed adsorption. This feature is confirmed by the LEED analysis described below.

LEED measurements were performed on a synthetic magnetite sample. The clean surface, prepared by  $\text{Ar}^+$ -ion sputtering and subsequent annealing at 900–1000 K at  $p_{\text{O}_2} = 5 \times 10^{-7}$  mbar for 2–3 h, exhibited a  $(\sqrt{2} \times \sqrt{2})R45^\circ$ -LEED pattern with sharp superstructure reflections and low background [Fig. 3(a)]. Water was adsorbed at 273 K for 2 min at a water vapor pressure of  $2 \times 10^{-6}$  mbar, resulting in a  $(1 \times 1)$ -LEED pattern with an enhanced background [Fig. 3(b)]. The latter is attributed to uncorrelated defects possibly induced by the electron beam [34]. However, the LEED  $I(V)$  curves remained unchanged during repeated measurements over periods of several hours. Annealing up to 770 K restores the superstructure spots but the shape of the LEED  $I(V)$  curves cannot be recovered, indicating some residual hydroxylation of the surface, as observed by Kendelewicz *et al.* [21]. Seven LEED  $I(V)$  curves of the  $(1 \times 1)$  surface were measured in the energy range 50–300 eV at 100 K.

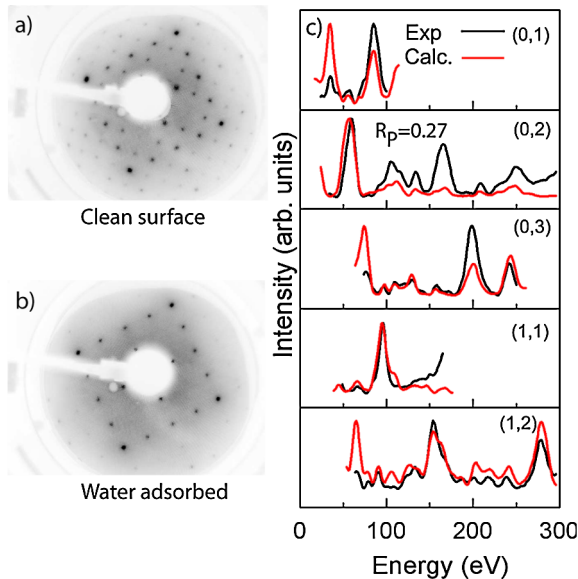


FIG. 3 (color online). LEED pattern (a) before and (b) after water adsorption. The superstructure spots in (a) indicative of the  $(\sqrt{2} \times \sqrt{2})R45^\circ$  surface reconstruction are largely suppressed in (b). (c) Experimental (averaged over symmetrically equivalent beams - black) and calculated [red (medium gray)] LEED  $I(V)$  curves of the water adsorbed surface.

LEED calculations were performed with the layer doubling method and a least squares optimization [35] using constraints for bond lengths. The crystal potential was calculated from a superposition of atomic potentials using optimized muffin-tin radii [36] which led to reliable structural determination of the clean  $\text{Fe}_3\text{O}_4(001)$  surface [19]. Ten phase shifts were used. All positions and occupation numbers within the adsorbate and top  $B$ - $A$ - $B$  substrate layers were optimized in a  $(\sqrt{2} \times \sqrt{2})R45^\circ$ -unit cell, while thermal parameters were kept fixed. The best fit ( $R_p = 0.27$ ) was obtained for a model where all  $\text{Fe}_B\text{S}$  sites have adsorbed oxygen on top. Both the surface  $\text{Fe}_B$  and adsorbate sites are occupied by  $\sim 80\%$  possibly due to defect creation during the preparation procedure. The adsorbed O shows strong lateral shifts by  $\sim 0.4$  Å off the  $\text{Fe}_B$  sites in agreement with the DFT results (0.23–0.28 Å). The main features are the two different bond lengths 2.12 Å ( $\text{Fe-O}^w$ ) and 1.93 Å ( $\text{Fe-O}^{\text{OH}}$ ), confirming the simultaneous occurrence of hydroxyl groups and molecular adsorption. Further details on the structural analysis will be published elsewhere.

We turn next to the surface and adsorbate induced electronic effects on  $\text{Fe}_3\text{O}_4(001)$ . The electron density plot in Fig. 4 displays the minority  $t_{2g}$  occupancies at the  $\text{Fe}_B$  sites, thus allowing us to distinguish between sites with predominant  $\text{Fe}^{2+}$  or  $\text{Fe}^{3+}$  character [29]. The notation  $\text{Fe}^{2+}$  and  $\text{Fe}^{3+}$  is used here for simplicity, but the difference in total  $3d$  occupation within the MT sphere is much smaller (0.2–0.4 $e$ ) consistent with x-ray diffraction [5] and LDA +  $U$  studies of the low temperature bulk phase [6,7]. The magnetic moments allow a clearer discrimination:  $M_{\text{Fe}^{2+}} = 3.54\text{--}3.75\mu_B$ ,  $M_{\text{Fe}^{3+}} = 3.90\text{--}4.10\mu_B$ , respec-

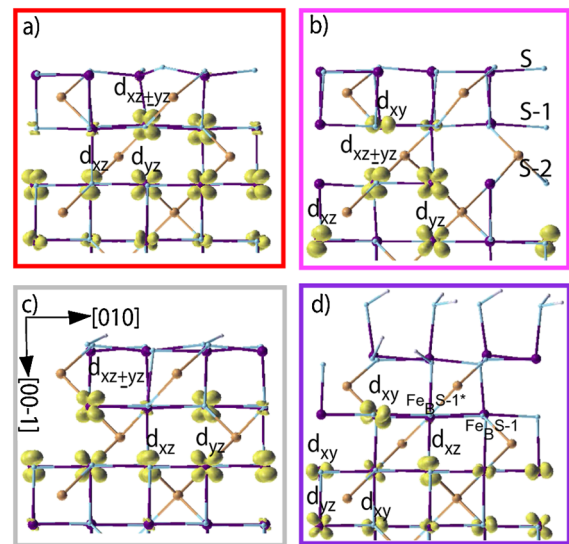


FIG. 4 (color online). Side view of the electron density integrated between  $-1.3$  eV and  $E_F$  showing the occupation of the minority  $t_{2g}$  orbitals at the  $\text{Fe}_B$  sites. (a)  $B + \text{V}_\text{O}$ ; (b)  $B$  layer; (c)  $B + \text{V}_\text{O} + 1\text{H}_2\text{O}(D)$ ; (d)  $B + 4\text{H}_2\text{O}(M)$ . For the color code see Fig. 1.

tively. For most of the stable systems we find that the surface layer contains exclusively  $\text{Fe}^{3+}$  while a unique charge and orbitally ordered state emerges in the deeper layers depending on the type of termination [37]. In  $B + V_O$  [Fig. 4(a)] the two subsurface  $\text{Fe}_B$  next to  $V_O$  are  $\text{Fe}^{2+}$  ( $d_{xz} \pm d_{yz}$ ). Upon water adsorption the positions of  $\text{Fe}^{2+}$  switch in  $B + V_O + 1\text{H}_2\text{O}(D)$ : now the two  $\text{Fe}_B$  below the surface OH groups are  $\text{Fe}^{2+}$ , resulting in alternating  $\text{Fe}^{2+}$ ,  $\text{Fe}^{3+}$  sites. In the mixed adsorption case ( $B + 4\text{H}_2\text{O}(M)$ ) the charge ordering in the subsurface layer is not significantly altered compared to the  $B$  layer, where one out of four  $\text{Fe}_B S-1$  is  $\text{Fe}^{2+}$  and a second is in an intermediate valence state. However, the slight tilting of the  $t_{2g}$  orbital at  $\text{Fe}_B^{2+}$  induces a completely different OO in  $S-2$ : from  $d_{xz} \pm d_{yz}$  to alternating  $d_{xy}$  and  $d_{xz}$ -orbitals. Recent GGA +  $U$  calculations have shown that in bulk magnetite a variety of CO/OO states can be realized by symmetry lowering [30]. Here the presence of a surface and adsorbates imposes a unique CO/OO state for each termination reaching several layers below the surface. Moreover, most of them violate the Anderson criterion:  $\text{Fe}_4\text{O}_4$  cubes in the surface and subsurface layer are predominantly electron poor ( $3\text{Fe}^{3+} + 1\text{Fe}^{2+}$ ), while those in the  $S-1$  and  $S-2$  layers are electron rich ( $1\text{Fe}^{3+} + 3\text{Fe}^{2+}$ ). Evidence for orbital ordering in thin magnetite films was reported recently from resonant soft x-ray diffraction [8].

The charge ordered state in the  $B$  layer leads to the opening of a band gap of 0.3 eV as shown in Fig. 2(d), consistent with previous calculations [18] and scanning tunneling spectroscopy measurements [38]. However, the adsorption of water on the surface and the formation of surface hydroxyl groups leads to half-metallic behavior.

We have shown that on  $\text{Fe}_3\text{O}_4(001)$  water tends to dissociate in oxygen vacancies or partially dissociate on the nondefective surface in contrast to the full dissociation found on  $\text{Fe}_3\text{O}_4(111)$  [21,39]. This adsorption mode is triggered by the presence of both Lewis acid and base sites on the surface and the intermolecular interaction as reported also on rutile(110) [40], anatase(001) [41], and  $\text{MgO}(001)$  surfaces [42]. The hydrogen-bonded OH and  $\text{H}_2\text{O}$  can easily rearrange and thus provide adsorption sites for further species (e.g., heavy metal complexes). Our results indicate a pathway to manipulate, e.g., the catalytic properties of transition metal oxide surfaces by triggering electron transfer processes and inducing new charge and orbitally ordered states via adsorbates.

We acknowledge discussions with G.E. Brown and T. Kendelewicz and support by the German Science Foundation (PE883/1-2) and a grant for computational time at the Leibniz Rechenzentrum Garching.

\*pentcheva@lrz.uni-muenchen.de

[1] Z. Zhang and S. Satpathy, Phys. Rev. B **44**, 13 319 (1991).  
[2] E.J.H. Verwey, Nature (London) **144**, 327 (1939).

- [3] J.H. Park *et al.*, Phys. Rev. B **55**, 12 813 (1997).  
[4] D. Schrupp *et al.*, Europhys. Lett. **70**, 789 (2005).  
[5] J.P. Wright, J.P. Attfield, and P.G. Radaelli, Phys. Rev. Lett. **87**, 266401 (2001).  
[6] I. Leonov *et al.*, Phys. Rev. Lett. **93**, 146404 (2004).  
[7] H.-T. Jeng, G.Y. Guo, and D.J. Huang, Phys. Rev. Lett. **93**, 156403 (2004).  
[8] J. Schlappa *et al.*, Phys. Rev. Lett. **100**, 026406 (2008).  
[9] K. Ohe *et al.*, J. Chem. Eng. Jpn. **38**, 671 (2005).  
[10] H. Katsumata *et al.*, J. Environ. Manage. **69**, 187 (2003).  
[11] C. Martos *et al.*, Int. J. Hydrogen Energy **34**, 4475 (2009).  
[12] M.A. Henderson, Surf. Sci. Rep. **46**, 1 (2002).  
[13] P.A. Thiel and T.E. Madey, Surf. Sci. Rep. **7**, 211 (1987).  
[14] P.W. Tasker, J. Phys. C **12**, 4977 (1979).  
[15] S.A. Chambers, S. Thevuthasan, and S.A. Joyce, Surf. Sci. **450**, L273 (2000).  
[16] B. Stanka *et al.*, Surf. Sci. **448**, 49 (2000).  
[17] R. Pentcheva *et al.*, Phys. Rev. Lett. **94**, 126101 (2005).  
[18] Z. Lodziana, Phys. Rev. Lett. **99**, 206402 (2007).  
[19] R. Pentcheva *et al.*, Surf. Sci. **602**, 1299 (2008).  
[20] M. Fonin *et al.*, Phys. Rev. B **72**, 104436 (2005).  
[21] T. Kendelewicz *et al.*, Surf. Sci. **453**, 32 (2000).  
[22] C.H.F. Peden *et al.*, Catal. Today **51**, 513 (1999).  
[23] J.R. Rustad, A.R. Felmy, and E.J. Bylaska, Geochim. Cosmochim. Acta **67**, 1001 (2003).  
[24] T.K. Kundu *et al.*, J. Colloid Interface Sci. **295**, 364 (2006).  
[25] P. Blaha *et al.*, WIEN2K, An Augmented Plane Wave + Local Orbitals Program for Calculating Crystal Properties (K. Schwarz, TU Wien, Austria, 2001).  
[26] J.P. Perdew *et al.*, Phys. Rev. Lett. **77**, 3865 (1996).  
[27] B. Santra *et al.*, J. Chem. Phys. **127**, 184104 (2007).  
[28] V.I. Anisimov *et al.*, Phys. Rev. B **48**, 16 929 (1993).  
[29] We have varied  $U$  between 0–8 eV: Charge disproportionation at the  $\text{Fe}_B$  sites is found beyond  $U = 2$  eV.  
[30] H.P. Pinto and S.D. Elliot, J. Phys. Condens. Matter **18**, 10427 (2006).  
[31] We have used muffin-tin (MT) radii of  $R_{\text{H}}^{\text{MT}} = 0.60$  Bohr,  $R_{\text{Fe}}^{\text{MT}} = 1.90$ , and  $R_{\text{O}}^{\text{MT}} = 1.10$ , an energy cutoff for the wave functions and potential of 25 Ry and 196 Ry, respectively, and 16  $k_{\parallel}$  points for the integration in the Brillouin zone.  
[32] K. Reuter and M. Scheffler, Phys. Rev. B **65**, 035406 (2001).  
[33] A clean or water adsorbed half-occupied  $A$  layer was found to be less stable in the pressure ranges studied here.  
[34] For a filament current of 50–100 nA a rough estimate of the electron dose is 1–2 (e/u.c.) per 10 s.  
[35] H. Over *et al.*, Phys. Rev. B **46**, 15 438 (1992).  
[36] J. Rundgren, Phys. Rev. B **68**, 125405 (2003).  
[37] Only for  $B + V_O$  a configuration with  $\text{Fe}^{2+}$  in the surface layer competes with the configuration in Fig. 4(a).  
[38] K. Jordan *et al.*, Phys. Rev. B **74**, 085416 (2006).  
[39] M.E. Grillo, M.W. Finnis, and W. Ranke, Phys. Rev. B **77**, 075407 (2008).  
[40] P.J.D. Lindan, N.M. Harrison, and M.J. Gillan, Phys. Rev. Lett. **80**, 762 (1998).  
[41] A. Vittadini *et al.*, Phys. Rev. Lett. **81**, 2954 (1998).  
[42] L. Giordano, J. Goniakowski, and J. Suzanne, Phys. Rev. Lett. **81**, 1271 (1998); M. Odelius, Phys. Rev. Lett. **82**, 3919 (1999).